J Mol Model (2013) 19:1919–1927
DOI 10.1007/s00894-013-1755-6

ORIGINAL PAPER

Computational design of glutamate dehydrogenase in *Bacillus subtilis* natto

Li-Li Chen · Jia-Le Wang · Yu Hu · Bing-Jun Qian · Xiao-Min Yao · Jing-Fang Wang · Jian-Hua Zhang

Received: 14 September 2012 / Accepted: 2 January 2013 / Published online: 22 January 2013

Abstract *Bacillus subtilis* natto is widely used in industry to produce natto, a traditional and popular Japanese soybean food. However, during its secondary fermentation, high amounts of ammonia are released to give a negative influence on the flavor of natto. Glutamate dehydrogenase (GDH) is a key enzyme for the ammonia produced and released, because it catalyzes the oxidative deamination of glutamate to alpha-ketoglutarate using NAD^+ or $NADP^+$ as co-factor during carbon and nitrogen metabolism processes. To solve this problem, we employed multiple computational methods model and re-design GDH from *Bacillus subtilis* natto. Firstly, a structure model of GDH with cofactor $NADP^+$ was constructed by threading and ab initio modeling. Then the substrate glutamate were flexibly docked into the structure model to form the substrate-binding mode. According to the structural analysis of the substrate-binding mode, Lys80, Lys116, Arg196, Thr200, and Ser351 in the active site were found could form a significant hydrogen bonding network with the substrate, which was thought to play a crucial role in the substrate recognition and position. Thus, these residues were then mutated into other amino acids, and the substrate binding affinities for each mutant were calculated. Finally, three single mutants (K80A, K116Q, and S351A) were found to have significant decrease in the substrate binding affinities, which was further supported by our biochemical experiments.

Keywords *Bacillus subtilis* natto · Glutamate dehydrogenase · Homology modeling · Rational design · Site-directed mutagenesis

L.-L. Chen · Y. Hu · B.-J. Qian · X.-M. Yao · J.-H. Zhang
Bor S. Luh Food Safety Research Center, Shanghai Jiao Tong University, Shanghai 200240, China

L.-L. Chen · B.-J. Qian · X.-M. Yao · J.-H. Zhang (✉)
Department of Food Science and Technology, Shanghai Jiao Tong University, Shanghai 200240, China
e-mail: zhangjh@sjtu.edu.cn

J.-L. Wang
School of Life Science and Biotechnology, Shanghai Jiao Tong University, Shanghai 200240, China

J.-F. Wang (✉)
Key Laboratory of Systems Biomedicine (Ministry of Education), Shanghai Jiao Tong University, Shanghai 200240, China
e-mail: jfwang8113@gmail.com

Introduction

Glutamate dehydrogenase (GDH) can be found in most microbes and the mitochondrial of eukaryotes, acting as the $NAD(P)^+$-linked oxidative deamination of L-glutamate to α-oxoglutarate. Mammalian GDH is able to utilize both NAD^+ and $NADP^+$, while those in plants or microbes can be specific for only one cofactor [1]. GDH links glutamate with the Krebs cycle and provides a major pathway for interconversion of amino acids and keto acids. In non-neural tissues, oxidation of glutamate by GDH is considered to be linked to the synthesis of ATP as an energy source. For their crucial functions, GDH and other members in the amino acid dehydrogenase enzyme family have commercial potentials in the production of novel non-proteogenic amino acids for the pharmaceutical industry [2–5].

Natto is a traditional and popular Japanese soybean product obtained by fermentation using *B. subtilis* natto, which has various bioactive properties such as prophylactic activity against venous thrombosis and osteoporosis [6–9]. However, during the secondary fermentation, high amounts of

ammonia are produced, which has a negative influence on the flavor of natto. The major metabolic pathways of ammonia production in bacteria are decarboxylation, trans-deamination, and transamination. GDH is significant in both trans-deamination and trans-amination.

B. subtilis strain r22 has two active glutamate dehydrogenase genes, *roc*G and *gud*B, and inactivating both genes reduced ammonia production by half [10]. However, the mutant strain grows much more slowly in nutrient broth medium or in a medium with glucose as the sole carbon source and glutamate as the sole nitrogen source [11]. Getting a strain with site-directed mutagenesis *gud*B gene and without *roc*G gene to retain partial GDH activity may be an alter strategy to reduce ammonia-releasing and maintain the growing ability.

To achieve this aim, molecular modeling was firstly employed to predict the three-dimensional structure of GDH from *B. subtilis* natto in situation of lacking X-ray or NMR structures in the related protein structure databases. Such approach has been widely used recently to solve biological problems, providing useful information for both basic research and drug development in the relevant areas [12–17]. Subsequently, the possible glutamate binding modes was predicted based on the structural model mentioned above. With these binding modes, the interactions of GDH with glutamate were analyzed, and the changes of binding free energy were calculated when key residues in the glutamate binding pocket were mutated to other amino acids. Finally, biological experiments were performed to verify enzyme reaction kinetics feature of these mutants.

Materials and methods

Strains, plasmids, and medium

The *B. subtilis* natto strain was isolated from commercial natto and identified by API 50 (BioMerieux, Inc., Marcy 1'Etoile, France). *E. coli* JM109 and DH5α were obtained from Takara (Dalan, China) and used as host strains for cloning and sequencing, respectively. *E. coli* BL21 (DE3) (Invitrogen, Shanghai, China) was used as a host strain for expression. The plasmid pMD19-T Simple Vector (Takara, Dalan, China) was used for cloning and sequencing, and the vector pET28a (Novagen) was used for expression. *E. coli* strains were grown in Luria-Bertani (LB) medium supplemented with kanamycin.

DNA manipulations

The *gudB* gene was amplified by polymerase chain reaction (PCR) with the genomic DNA of *B. subtilis* natto as template. To identify the *gud*B region, the relevant forward and reverse primers (5′-GCCTGCAAGAGTATGGTAAG-3′, and 5′-GATAGTCCACAAGGTCCTCC-3′) were designed based on the published sequence of the *gud*B gene of *B. subtilis* strain 168. Methods for plasmid isolation, agarose and polyacrylamide gel electrophoresis (PAGE), uses of restriction enzymes, ligase, and DNA modification enzymes, PCR, and electroporation of *E. coli* JM109 cells were performed as described by Sambrook et al. [18]. The cloning gene was sequenced by Sunny Bio. (Shanghai, China).

Molecular modeling

To construct the three-dimensional structure of GDH from *B. subtilis* natto, eight threading programs (SAM [19], SPARKS [20], FUGUE [21], COMA [22], HHSEARCH [23], PROSPECT [24], SP3 [25] and MUSTER [26]) were employed to search for structural templates having high sequence or structural similarities with the target protein. Finally, five structures (1gtm.pdb, 1bgv.pdb, 1b26.pdb, 2bma.pdb and 1euz.pdb) were identified from the RCSB Protein Data Bank (PDB) [27] as structural templates to construct the computational model of GDH from *B. subtilis* natto. Segment matching or coordinate reconstruction [28–32] was used as the computational approach to predict the aligned region structures, and ab initio modeling was employed for constructing the unaligned region structures of the target proteins [32, 34]. The coordinate reconstruction processes were done by the homology module in MOE 2008 [34]. After a series of molecular dynamics simulations, the computational three-dimensional structure of GDH from *B. subtilis* natto was obtained, which was further assessed by PROCHECK [35] and QMEAN [36].

Molecular docking procedure

Based on the computational model obtained from the molecular modeling approach, molecular docking operations were carried out with Monte Carlo simulated annealing [37] to get the favorable binding modes for GDH with the substrate glutamate. As ligand binding in the active site may induce some conformational changes, a flexible docking procedure was adopted to construct the binding modes. Before the docking procedure, 10,000 configurations of GDH were extracted from short-time molecular dynamics simulations (~1 ns). The ligand was then docked into all these configurations to search for the favorable binding modes. The docking program (docking module in MOE 2008 [34]) used in the current study would automatically generate a diversified set of configurations by randomly altering the atomic coordinates of the ligand. Then, the search for the favorable binding mode for each configuration was performed within a specified three-dimensional

box by simulated annealing to optimize the purely spatial contacts as well as electrostatic interactions. Finally, the favorable binding mode thus obtained was further optimized by a series of short molecular dynamics simulations. During the docking procedure, the Merck force field parameters were adopted, and the binding modes were assessed by a scoring function London dG which was successfully used in other theoretical studies [38].

Molecular dynamics simulations

The molecular dynamics simulations mentioned above were performed by GROMACS 4.0 [39] with GROMACS force field parameters, periodic boundary condition and NPT ensemble. The initial models were solvated in a specific simulation box with SPC water molecules and a space of 10 Å around the solute. To neutralize the redundant changes, some sodiums or chloridions were added to the simulation systems, which were then subjected to a 2000-step energy minimization with the steepest descents approach. Finally, 10 ns molecular dynamics simulations were performed at 298 K. During all the simulations, all the chemical bonds were constrained by the LINCS algorithm, and the atom velocities for start-up runs were obtained according to a Maxwell distribution at 298 K. To maintain the simulation systems at a constant temperature and pressure, the Berendsen thermostat was applied with a coupling time of 0.1 and 1.0 ps. The particle mesh Ewald (PME) algorithm was employed to treat electrostatic interactions with interpolation order of 4.0 and a grid spacing of 0.12. The van der Waals interactions were treated by using a cutoff of 12 Å. The integration step was set to be 2.0 fs, and the coordinates were saved every 1 ps.

Site-directed mutagenesis

Mutagenesis was performed using the quick-change lightning site-directed mutagenesis kit (Stratagene), and *gud*B was used as a template for PCR amplification. Synthetic oligonucleotide primer pairs (Sangon Biotech, Shanghai) for the mutants of K80A, K116Q, and S351A were listed in Table 1, and the mutated codons were underlined. Following temperature cycling, the product was treated with Dpn I (Fermentas). The presence of mutations was confirmed by DNA sequencing (Sunny Biotech, Shanghai). The DNAs containing the desired mutations cloned with plasmid vectors were transformed into *E. coli* XL10-Gold ultracompetent cells. This site-directed mutagenesis procedure was similar to the method described by Rigoni et al. [40, 41]. The *gud*B gene mutants K80A, K116Q, and S351A were used as templates for further PCR amplification to get the double-site and multiple-site mutants, K80A/K116Q, K80A/S351A, K116Q/S351A, and K80A/K116Q/S351A.

Protein overexpression and purification

The sequences of the forward and reverse primers were 5′-CGTACGGCTAGCATGGCGGCCGATCGAAAC-3′ and 5′-CGCTAGGAATTCCGATTGGCATTTCACTTT-3′, respectively. The forward primer contained a *Nhe*I recognition site (GCTAGC) and the reverse primer contained an *Eco*RI recognition site (GAATTC) for convenient subcloning into the pET28a vector. PCR amplification was performed in a 50 μl reaction mixture with 1U of Pyrobest DNA polymerase (Takara). The PCR product was purified (PCR clean-up kit, Generay), digested with *Nhe*I and *Eco*RI, and ligated into the pET28a vector using T4 DNA ligase (Fermentas). The obtained plasmid constructs were transformed into the expression strain *E. coli* BL21 (DE3). All constructs were verified by sequencing of the plasmid DNA.

The purification of the His-tagged protein from isopropyl β-D-thiogalactoside (IPTG)-induced *E. coli* BL21 (DE3) cells containing pET28a/GDH (either wild-type or mutations) was performed according to the standard procedure of the manufacturer (Qiagen). Refolding was initiated by dilution of the eluted protein into a buffer containing 4 % PEG 4000, 20 mM oxidized glutathione, and 40 mM reduced glutathione. After refolding, the solution was dialyzed with TE buffer (pH7.2).

Enzyme kinetics assay and protein determination

The enzyme activity and K_m assay for GDH involving deamination reaction was performed in 3 ml of 25 mM Tris-HCl buffer (pH8.5) containing various concentrations (50, 40, 30, 20, and 10 mM) of L-glutamate, and 0.5 mM $NADP^+$ at 25 °C. When NAD^+ was used as coenzyme, the

Table 1 Detailed information for the synthetic mutagenic primers

K80A	Forward	5′-GTGAAAACGTATCCCGCCT**GC**CGTTACCGACAGAG-3′
	Reverse	5′-CTCTGTCGGTAACG**GC**AGGAGGGATACGTTTCAC-3′
K116Q	Forward	5′-GGATCACAAACAATTCCGCCT**TG**ACCACCGCCATAT-3′
	Reverse	5′-ATAGGCGGTGGT**C**AAGGCGGAATTGTTTGTGATCC-3′
S351A	Forward	5′-AACTGTTACGCCACCGGCA**GC**TGCCAGCAGC-3′
	Reverse	5′-GCTGCTGGCA**GC**TGCCGGTGGCGTAACAGTT-3′

reaction was performed in 3 ml of 160 mM glycine buffer (160 mM glycine, 1.8 M NaCl, 4.2 mM EDTA, pH9.0) [42] with various concentrations of L-glutamate as described above and 6 mM NAD^+ at 25 °C. The increase in NADPH or NADH was measured kinetically at 340 nm using a Beckman Coulter DU800 spectrophotometer. One unit of enzyme activity was defined as the amount of enzyme catalyzing the reaction of 1 μmol of $NADP^+$ or NAD^+ per minute at 25 °C. All experiments were performed independently at least three times. K_m value was determined from Lineweaver-Burk plots with the initial reaction rate. The protein concentration was calculated by measuring the absorbance of the protein solution at 280 nm and 260 nm.

Results and discussion

Computational models

The most popular approaches for prediction protein three-dimensional structure are homology modeling and threading. However the most important procedure for both methods is how to identify the structural template which has highly similarity on sequences or structures with the target proteins. To this end, eight popular methods (SAM [19], SPARKS [20], FUGUE [21], COMA [22], HHSEARCH [23], PROSPECT [24], SP3 [25] and MUSTER [26]) were employed to search the PDB for finding template structures for GDH. Five structures (1gtm.pdb, 1bgv.pdb, 1b26.pdb, 2bma.pdb, and 1euz.pdb) were thus identified, and multiple sequence alignments were performed on the template and target proteins. As shown in Fig. 1, the sequence similarity scores of the target protein with its template structures were 54 %, 30 %, 50 %, 28 %, and 50 %, respectively. Based on the sequence alignment results and the template structures, the aligned regions of GDH were constructed by the threading approach. For the unaligned regions, the ab initio approach was employed to build the corresponding structures. Thus, the entire three-dimensional structure of GDH from *B. subtilis* natto was obtained (Fig. 2a).

To validate our computational model, multiple methods were employed to estimate the local and global model quality, stereochemistry, as well as structural features for our computational structure of GDH. The local model quality, which was estimated by ANOLEA [43] in Swiss Model Workspace, indicated that most residues in our model were located in the favorable areas. QMEAN is a scoring function of a linear combination of six structural descriptors: Cβ interaction energy, all-atom pairwise energy, salvation energy, torsion angle energy, secondary structure, and solvent

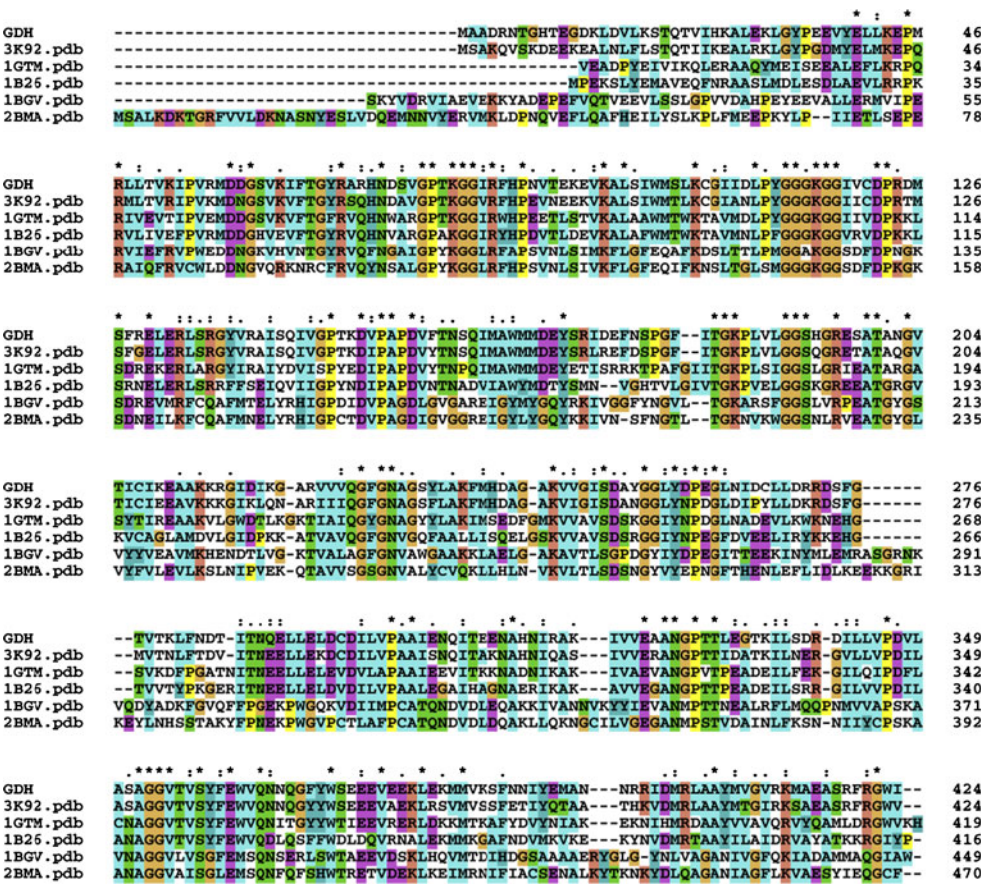

Fig. 1 The multiple sequence alignment of the target protein with its template structures. The target protein is GDH from *B. subtilis* natto; the structural templates are 1gtm.pdb, 1bgv.pdb, 1b26.pdb, 2bma.pdb as well as 1euz.pdb. The sequence similarity scores of the target protein with these templates are 54 %, 30 %, 50 %, 28 %, and 50 %, respectively

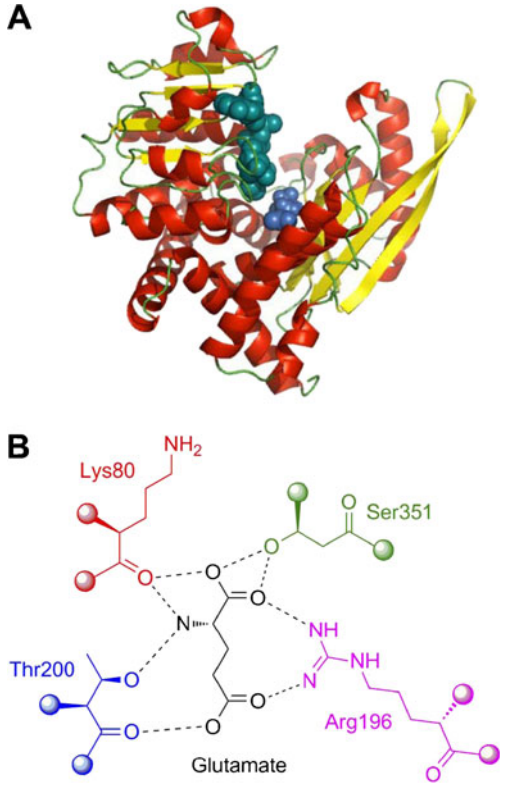

Fig. 2 The three-dimensional computational structure for GDH from *B. subtilis* natto. **a** The overall structure of the computational model with cofactor $NADP^+$ and substrate glutamate. Only backbone structure of the computational model is shown, and the cofactor and substrate are colored in *green* and *blue*, respectively. **b** 2D hydrogen bonding interactions between the residues in the active and substrate glutamate. The key residues Lys80, Arg196, Thr200, and Ser351 are colored in *red*, *pink*, *blue*, and *green*, respectively

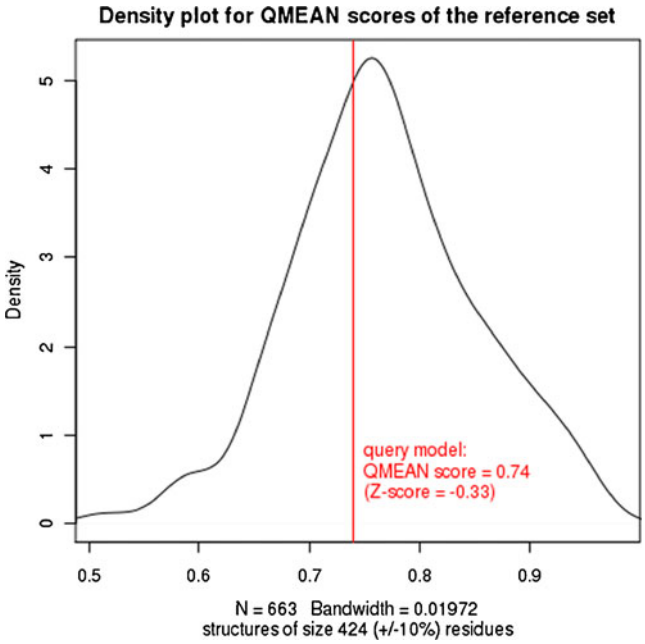

Fig. 3 The density plot of the QMEAN score for the computational model of GDH from *B. subtilis* natto. QMEAN score is a scoring function of a linear combination of Cβ interaction energy, all-atom pairwise energy, salvation energy, torsion angle energy, secondary structure, and solvent accessibility. This score ranges between 0 and 1, the higher value to reflect the better quality of the model. In the current case, QMEAN score for our computational model was 0.74

accessibility [36]. The QMEAN score ranges between 0 and 1, the higher value, reflect the better quality of the model. The score of the local model quality was 0.74, its density plot was shown in Fig. 3. To evaluate the absolute model quality, a Z score of the computational model was further calculated in comparison with the scores of the reference X-ray structures of similar size from the PDB (Fig. 4).

The global model quality was assessed by DFIRE [44], an all-atom statistical potential based on a distance-scaled finite ideal-gas reference state. This approach was used to assess non-bonded atomic interactions in the protein model, and pseudo energies for the computational model. The DFIRE result for our computational model is −588.20, indicating that the model was close to the native conformation. The stereochemistry features were checked by PROCHECK package [35], and the results showed that 92.1 % residues of the computational model were located in the core region, 6.0 % in the allowed region, 1.1 % in the general region, and only 0.8 % in the disallowed region (Fig. 5). Additionally, for the main-chain residues, 99.8 % of the bond lengths and 93.6 % of the bond angles were within the allowed limits. For a good quality model, the residues located in the core regions should be expected to be more than 90 %. All these findings indicated that our

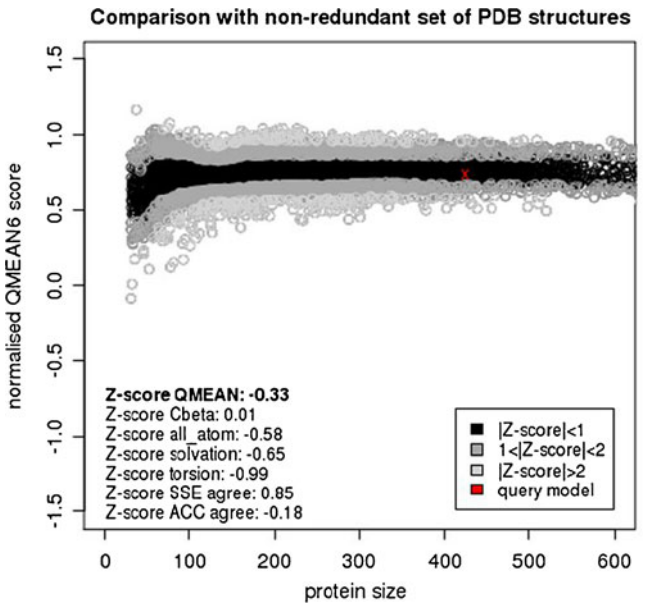

Fig. 4 Estimated absolute model quality by the comparison of the QMEAN scores with the reference X-ray structures in the Protein Data Bank. A Z-score is used to estimate the absolute model quality of the computational model, which gives a direct indication that the computational model is quite reliable

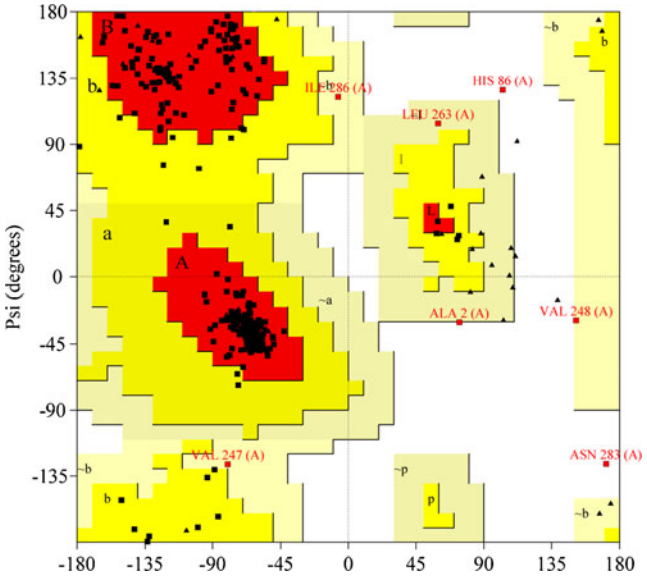

Fig. 5 The PROCHEKC report for the computational model of GDH from B. subtilis natto. For a good quality model, the residues located in the core regions should be expected to be more than 90 %. In the current case, 92.1 % residues of the computational model were located in the core region, 6.0 % in the allowed region, 1.1 % in the general region, and only 0.8 % in the disallowed region

computational three-dimensional structure of GDH from *B. subtilis* natto was quite reliable.

Substrate binding analysis

The overall structure of the computational model was quite similar to the crystal structures of the bacterial and animal forms of GDH, which showed two-trimer architectures with subunits stacked directly on top of each other [45–49]. The computational structure, as well as the subunit in the crystal structures, was considered to be composed of at least three domains. According to the crystal report, the bottom domain of the subunit made extensive contacts with another one from the other trimer. Resting on top of this domain is the cofactor binding domain that employed the conserved nucleotide binding motif. Some GDH also had a long protrusion called antenna, rising above the cofactor binding domain. However antenna is unique for animals, and not detected in bacteria, plants, fungi, and the vast majority of protists. In animal GDH, the antenna domain located immediately behind the adjacent, counterclockwise neighbor within the trimer. This part of GDH usually appeared in the enzymes that were reported to be allosterically regulated by a series of ligands. Thus, it is reasonable to speculate that antenna domain played an important role in regulation.

Based on the aforementioned computational structure of GDH and multiple sequence alignment, the potential binding sites of the cofactor and substrate (glutamate) were identified based on the crystal studies. The identified binding site for the cofactor $NADP^+$ was composed of residues 200, 227–232, 251–253, 302–304 and 324–326, which was similar with the crystal structure 1v9i.pdb [50] and 3mw9.pdb [46]. The binding position of the substrate was identified to be located on the residues 80–82, 101, 104, 116, 154–156, 196–203, 326, 354, 355 and 358, which was supported by the crystal studies in other GDH enzymes (3ete.pdb) [51]. Upon the aforementioned information, the substrate was docked into the identified binding site using comparatively flexible docking procedure, and the most favorable binding mode for both cofactor and substrate was selected and shown in Fig. 2a. The result showed that the substrate (glutamate) was fixed in the active site of the enzyme by a significant hydrogen bonding network formed by Lys80, Lys116, Arg196, Thr200, and Ser351. To estimate the hydrogen bonding interactions, the hydrogen bond lifetime for all the configurations in our docking procedure was calculated (Table 2), and the detailed information for the ones that employed comparatively high life-time were shown in Fig. 2b. The hydrogen bond with a life-time more than 10 % was believed to be stable during the entire simulations and to have strong interactions with the substrate. Interestingly, these results were also found to be located in highly conserved regions of GDH.

Thus, in order to reduce the activity of GDH, it was reasonable to mutate the residues having important hydrogen bonding interactions with the substrate. Thus, the residues in the active site, which can form hydrogen bond having a life-time of more than 10 % with the substrate, were selected and mutated into another 19 amino acids. London dG, a scoring function implemented in molecular operating environment (MOE), was successfully used to calculate the binding affinities of proteins and ligands in the previous theoretical studies [40]. It was applied to assess the substrate binding affinities for all the mutants. Finally, three single mutants (S80A, K116Q, and S351A) were screened to employ significant decrease in the substrate binding affinities.

Experimental validation

To further confirm the computational results, biological experiments were performed. Single mutants (K80A, K116Q, and

Table 2 The hydrogen bond (life-time>10 %) information between GDH and its substrate glutamate

Residues	Life-time (%)	Residues	Life-time (%)
Lys80	62	Asn326	16
Arg196	50	Asp156	15
Thr200	41	Pro155	14
Ser351	29	Lys104	11
Lys116	26	Ser358	10

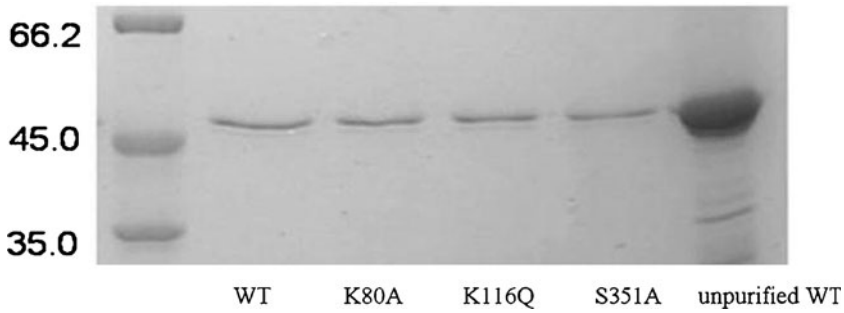

Fig. 6 SDS-PAGE analysis of the purified protein

Ser351A) as well as their double mutants (K80A/K116Q, K80A/S351A, and K116Q/S351A) and multiple mutants (K80A/K116Q/S351A) were constructed for the further PCR-based mutagenesis. The resulting circular plasmids containing the point mutations were verified by gene sequencing. Occasionally, a frame-shift mutant with an extra T inserted between cDNA position 363 and 364 was obtained by PCR-based mutagenesis. This plasmid was used as negative control in experiments of expressing the enzymes in *E. coli* and assaying for the enzyme activities.

The recombinant plasmids pET28a/GDH (wild-type and all the mutants) were used for transformation into *E.coli* BL21 (DE3). Genes cloned into these expression vectors were transcribed from the T7 promoter by T7 polymerase. The gene expressing T7 polymerase is presented in the chromosomes of *E.coli* BL21 (DE3), and the enzyme expression via the *lac* promoter can be induced by IPTG. Sodium dodecyl sulfate (SDS) gel electrophoresis of the induced cultures revealed a very strong band corresponding to an approximate relative molecular mass of 47 kDa in the insoluble factions. These results showed a good agreement with the values calculated from the deduced amino acid sequences (45.6 kDa). This band was absent in the samples from the control cells, which contained the pET28a plasmid without the inserted gene. After elution from a nickel-nitrilotriacetic acid (Ni-NTA) column, SDS gel electrophoresis of all eluted fractions contained only one band with a size of approximately 47 kDa (Fig. 6).

Expression in *E. coli* allows large-scale production of proteins. However, the requirement of proteins with normal activity and stability is a major difficulty in developing protein-overexpressing systems in *E. coli*. In the current case, the overexpressed protein formed inclusion bodies. After purification by Ni-NTA column, the enzymes were refolded by dilution to obtain proteins with normal activities.

The purified and refolded enzymes obtained in the present study showed oxidative deamination activity with either $NADP^+$ or NAD^+ as cofactor. When $NADP^+$ was used as a cofactor, the K_m values of the single mutants K80A, K116Q, and S351A increased to 44 mM, 41 mM, and 40 mM, respectively, while the K_m value for the wild-type enzyme was 23 mM (Table 3). However, the V_{max} values, which for the wild-type enzyme was 0.029 U min^{-1}, for these single mutants decreased to 0.020 U min^{-1}, 0.019 U min^{-1}, and 0.016 U min^{-1}, respectively. For the double mutants K80A/K116Q, K80A/S351A, and K116Q/S351A and multiple mutants K80A/K116Q/S351A, the corresponding K_m values were detected to be 115 mM, 77 mM, 81 mM, and 104 mM, respectively (Table 3). The V_{max} for these mutants were detected to be 0.020 U min^{-1}, 0.015 U min^{-1}, 0.016 U min^{-1}, and 0.013 U min^{-1}, respectively. The enzyme activities were significantly different between WT and mutants. When NAD^+ was selected as a cofactor, the K_m values of the single mutants increased to 80 mM, 95 mM, and 88 mM,

Table 3 Kinetic parameters for native and recombinant GDH determined for the deamination reaction with either NADP or NAD as cofactor

Enzymes	NADP			NAD		
	Vmax (U min^{-1})	Kmax (mM)	V/K	Vmax (U min^{-1})	Kmax (mM)	V/K
WT	0.029±0.002	22.6±1.3	1.29±0.07	0.065±0.001	77.2±3.1	0.85±0.03
K80A	0.020±0.001	44.4±1.8	0.46±0.03	0.030±0.001	80.0±2.5	0.37±0.01
K116Q	0.019±0.001	40.8±2.5	0.45±0.01	0.026±0.001	95.4±1.9	0.27±0.01
S351A	0.016±0.001	39.7±0.9	0.40±0.01	0.021±0.001	88.5±2.3	0.23±0.00
K80A/K116Q	0.020±0.001	115±8.2	0.17±0.01	0.018±0.001	108±3.6	0.17±0.01
K80A/S351A	0.015±0.001	77.0±3.1	0.19±0.01	0.015±0.002	92.0±2.7	0.16±0.01
K116Q/S351A	0.016±0.001	80.9±3.8	0.20±0.01	0.013±0.001	94.8±1.4	0.14±0.01
K80A/K116Q/S351A	0.013±0.001	104±5.7	0.13±0.01	0.014±0.001	105±9.3	0.13±0.01

respectively. For the double mutants and multiple mutants, the K_m values were detected to be 108 mM, 92 mM, 95 mM, 105 mM, respectively (Table 3).

Conclusions

Glutamate dehydrogenase is the branch-point enzyme of most importance during carbon and nitrogen metabolism for most microbes and the mitochondrial of eukaryotes. GDH from *Bacillus subtilis* natto is found to have significant influence on ammonia produce during the natto fermentation. In the current study, multiple computational methods were employed to redesign GDH from *B. subtilis* natto, with an aim to find a novel enzyme to improve the natto taste. Using threading and ab initio modeling approach, a three-dimensional structural model of GDH with cofactor $NADP^+$ and substrate glutamate docked into the active site was constructed. By further structural analysis, the residues in the active site were detected to form a significant hydrogen bonding network with the substrate glutamate, which was considered to play a crucial role for the substrate binding. Then, the residues which can form hydrogen bond having a life-time of more than 10 % with the substrate, were selected and mutated, and the substrate binding affinities were re-calculated. Finally, three single mutants (K80A, K116Q, and S351A) were screened to employ significant decrease in the substrate binding affinities. These computational results were further confirmed by mutagenesis experiments, which showed that the single mutants, as well as their double and multiple mutants could effectively reduce the activities of GDH.

Acknowledgments This work was supported by the grants from National Natural Science Foundation of China (No. 31171737 and 31200547) and Doctoral Program Foundation of Institutions of Higher Education of China (No. 20090073120079 and 2011073120078).

References

1. Hudson RC, Daniel RM (1993) L-glutamate dehydrogenates: distribution, properties and mechanism. Comp Biochem Physiol B 106:767–792
2. Hanson RL, Singh J, Kissick TP, Patel RN, Szarka LJ, Mueller RH (1990) Synthesis of L-β-hydroxyvaline from α-keto-β-hydroxyisovalerate using leucine dehydrogenase from Bacillus species. Bioorg Chem 18:116–130
3. Dooley KC (1992) Enzymatic methods for phenylketonuria screening using phenylalanine dehydrogenase. Clin Biochem 25:271–275
4. Livesey G, Lund P (1988) Determination of branched-chain amino and keto acids with leucine dehydrogenase. Methods Enzymol 166:3–10
5. Wendel U, Hummel W, Langenbeck U (1989) Monitoring of phenylketonuria: a colorimetric method for the determination of plasma phenylalanine using L-phenylalanine dehydrogenase. Anal Biochem 180:91–94
6. Yamaguchi M, Taguchi H, Gao Y, Igarashi A, Tsukamoto Y (1999) Effect of vitamin K2 (menaquinone-7) in fermented soybean (natto) on bone loss in ovariectomized rats. J Bone Miner Metab 17:23–29
7. Yamashita T, Oda E, Giddings J, Yamamoto J (2004) The effector of dietary bacillus natto productive protein on in vivo endogenous thrombolysis. Pathophysiol Heamost Thromb 33:138–143
8. Tsukamoto Y, Kasai M, Kakuda H (2001) Construction of a Bacillus subtilis (natto) with high productivity of vitamin K2 (menaquinone-7) by analog resistance. Biosci Biotechnol Biochem 65:2007–2015
9. Iwai K, Nakaya N, Kawasaki Y, Matsue H (2002) Antioxidative functions of natto, a kind of fermented soybeans: effect on LDL oxidation and lipid metabolism in cholesterol-fed rats. J Agric Food Chem 50:3597–3601
10. Kada S, Yabusaki M, Kaga T, Ashida H, Yoshida K (2008) Identification of two major ammonia-releasing involved in secondary natto fermentation. Biosci Biotechnol Biochem 72:1869–1876
11. Belitskey B, Sonenshein A (1998) Role and regulation of Bacillus subtilis glutamate dehydrogenase genes. J Bacteriol 180:6298–6305
12. Lian P, Wei DQ, Wang JF, Chou KC (2011) An allosteric mechanism inferred from molecular dynamics simulations on phospholamban pentamer in lipid membranes. PLoS One 6:e18587
13. Wang JF, Chou KC (2011) Insights from modeling the 3D structure of New Delhi metallo-β-lactamse and its binding interactions with antibiotic drugs. PLoS One 6:e18414
14. Wang Y, Wei DQ, Wang JF (2010) Molecular dynamics studies on T1 lipase: insight into a double-flap mechanism. J Chem Inf Model 50:875–878
15. Wang JF, Chou KC (2012) Insights into the mutation-induced HHH syndrome from modeling human mitochondrial ornithine transporter-1. PLoS One 7:e31048
16. Li J, Wei DQ, Wang JF, Li YX (2011) A negative cooperativity mechanism of human CYP2E1 inferred from molecular dynamics simulations and free energy calculations. J Chem Inf Model 51:3217–3225
17. Wang JF, Wei DQ, Chen C, Li Y, Chou KC (2008) Molecular modeling of two CYP2C19 SNPs and its implications for personalized drug design. Protein Pept Lett 15:27–32
18. Sambrook J, Russell D Molecular cloning: a laboratory manual. Cold Spring Harbor Laboratory Press, Cold Spring Harbor
19. Karplus K, Katzman S, Shacklefor G, Koeva M, Draper J, Barnes B, Sorinao M, Hughey R (2005) SAM-T04: what is new in protein-structure prediction for CASP6. Proteins 61:135–142
20. Zhou H, Zhou Y (2004) Single-body residue-level knowledge-based energy score combined with sequence-profile and secondary structure information for fold recognition. Proteins 55:1005–1013
21. Shi J, Blundell TL, Mizuguchi K (2001) FUGUE: sequence-structure homology recognition using environment-specific substitution tables and structure-dependent gap penalties. J Mol Biol 310:243–257
22. Margelevicius M, Venclovas C (2010) Detection of distant evolutionary relationships between protein families using theory of sequence profile–profile comparison. BMC Bioinforma 11:89
23. Soding J (2005) Protein homology detection by HMM–HMM comparison. Bioinformatics 21:951–960
24. Xu Y, Xu D (2000) Protein threading using PROSPECT: design and evaluation. Proteins 40:343–354
25. Zhou H, Zhou Y (2005) Fold recognition by combining sequence profiles derived from evolution and from depth-dependent structural alignment of fragments. Proteins 58:321–328

26. Wu S, Zhang Y (2008) MUSTER: improving protein sequence profile–profile alignments by using multiple sources of structure information. Proteins 72:547–556
27. Berman HM, Westbrook J, Feng Z, Gilliland G, Bhat TN, Weissig H, Shindyalov IN, Bourne PE (2000) The Protein Data Bank. Nucleic Acids Res 28:235–242
28. Wang JF, Wei DQ, Li L, Zheng SY, Li YX, Chou KC (2007) 3D structure modeling of cytochrome P450 2C19 and its implication for personalized drug design. Biochem Biophys Res Commun 355:513–519. Erratum in: Biochem Biophys Res Commun 2007, 357:330. Biochem Biophys Res Commun 2009, 384:399
29. Chen Q, Zhang T, Wang JF, Wei DQ (2011) Advances in human cytochrome P450 and personalized medicine. Curr Drug Metab 12:436–444
30. Blundell TL, Sibanda BL, Sternberg MJE, Thornton JM (1987) Knowledge-based prediction of protein structures and design of novel molecules. Nature 326:347–352
31. Zeng QK, Du HL, Wang JF, Wei DQ, Wang XN, Li YX, Lin Y (2009) Reversal of coenzyme specificity and improvement of catalytic efficiency of Pichia stipitis xylose reductase by rational site-directed mutagenesis. Biotechnol Lett 31:1025–1029
32. Wu S, Skolnick J, Zhang Y (2007) Ab initio modeling of small proteins by iterative TASSER simulations. BMC Biol 5:17
33. Wang JF, Zhang CC, Wei DQ, Li YX (2010) Docking and molecular dynamics Studies on CYP2D6. Chinese Sci Bull 55:1877–1880
34. Chemical Computing Group Inc (2012) Molecular operating environment (MOE) Chemical Computing Group Inc. Montreal, QC, Canada
35. Laskowski RA, MacArthur MW, Moss D, Thornton JM (1993) PROCHECK: a program to check the stereochemical quality of protein structures. J Appl Crystallogr 26:283–291
36. Benkert P, Tosatto SC, Schomburg D (2008) QMEAN: a comprehensive scoring function for model quality assessment. Proteins 71:261–277
37. Chou KC, Carlacci L (1991) Simulated annealing approach to the study of protein structures. Protein Eng 4:661–667
38. Morris GM, Goodsell DS, Halliday RS, Huey R, Hart WE, Belew RK, Olson AJ (1998) Automated docking using a Lamarckian genetic algorithm and an empirical binding free energy function. J Comput Chem 19:1639–1662
39. van der Spoel D, Lindahl E, Hess B, Groenhof G, Mark AE, Berendsen HJC (2005) GROMACS: fast, flexible, and free. J Comput Chem 26:1702–1718
40. Labute P (2008) The generalized Born/volume integral implicit solvent model: estimation of the free energy of hydration using London dispersion instead of atomic surface area. J Comput Chem 29:1693–1698
41. Rigoni M, Caccin P, Johnson E, Montecucco C, Rossetto O (2001) Site-directed mutagenesis identifies active-site residues of the light chain of botulinum neurotoxin type A. Biochem Biophys Res Commun 288:1231–1237
42. Nakasako M, Fujisawa T, Adachi S, Kudo T, Higuchi S (2001) Large-scale domain movements and hydration structure changes in the active-site cleft of unligated glutamate dehydrogenase from Thermococcus profundus studied by cryogenic X-ray crystal structure analysis and small-angle X-ray scattering. Biochemistry 40:3069–3079
43. Melo F, Feytmans E (1998) Assessing protein structures with a non-local atomic interaction energy. J Mol Biol 277:1141–1152
44. Zhou H, Zhou Y (2002) Distance-scaled, finite ideal-gas reference state improves structure-derived potentials of mean force for structure selection and stability prediction. Protein Sci 11:2714–2726
45. Baker PJ, Britton KL, Engel PC, Farrants GW, Lilley KS, Rice DW, Stillman TJ (1992) Subunit assembly and active site location in the structure of glutamate dehydrogenase. Proteins 12:75–86
46. Peterson PE, Smith TJ (1999) The structure of bovine glutamate dehydrogenase provides insights into the mechanism of allostery. Structure 7:769–782
47. Smith TJ, Schmidt T, Fang J, Wu J, Siuzdak G, Stanley CA (2002) Crystal structure of HsIUV complexed with a vinyl sulfone inhibitor: corroboration of a proposed mechanism of allosteric activation of HsIV by HsiU. J Mol Biol 318:765–777
48. Smith TJ, Peterson PE, Schmidt T, Fang J, Stanley CA (2001) Structures of bovine glutamate dehydrogenase complexes elucidate the mechanism of purine regulation. J Mol Biol 307:707–720
49. Banerjee S, Schmidt T, Fang J, Stanley CA, Smith TJ (2003) Structural studies on ADP activation of mammalian glutamate dehydrogenase and the evolution of regulation. Biochemistry 42:3446–3456
50. Bhujya MW, Sakuraba H, Ohshima T, Imagawa T, Katunuma N, Tsuge H (2005) The first crystal structure of hyperthermostable NDA-dependent glutamate dehydrogenase from Pyrobaculum islandicum. J Mol Biol 345:325–337
51. Li M, Smith CJ, Walker MT, Smith TJ (2009) Novel inhibitors complexed with glutamate dehydrogenase: allosteric regulation by control of protein dynamics. J Biol Chem 284:22988–223000